JOURNAL OF GEOPHYSICAL RESEARCH, VOL. 95, NO. D11, PAGES 18,641-18,652, OCTOBER 20, 1990

Kelvin Wave-Induced Trace Constituent Oscillations in the Equatorial Stratosphere

WILLIAM J. RANDEL

National Center for Atmospheric Research, Boulder, Colorado

Kelvin wave induced oscillations in ozone (O_3), water vapor (H_2O), nitric acid (HNO_3) and nitrogen dioxide (NO_2) in the equatorial stratosphere are analyzed using Limb Infrared Monitor of the Stratosphere (LIMS) data. Power and cross-spectrum analyses reveal coherent eastward propagating zonal wave 1 and 2 constituent fluctuations, due to the influence of Kelvin waves previously documented in the LIMS data. Comparison is made between a preliminary and the archival versions of the LIMS data (denoted V4 and V5, respectively); significant differences are found, demonstrating the sensitivity of constituent retrievals to derived temperature profiles. Because Kelvin waves have vanishing meridional velocity, analysis of tracer transport in the meridional plane is substantially simplified. Kelvin wave vertical advection is demonstrated by coherent, in-phase temperature-tracer oscillations, co-located near regions of strong background vertical gradients. Regions of out-of-phase coherency between temperature and trace species are also observed which suggest temperature dependent photochemistry. The temperature-ozone signatures in LIMS data are compared with a simple analytical model incorporating transport and photochemistry, and overall good agreement is found. These analyses provide a good cross-check on the quality of satellite constituent retrievals in the tropics, and also allow simple testing of chemical model parameterization schemes.

1. INTRODUCTION

A significant fraction of the space-time variance in tropical zonal wind and temperature fields is observed to be contained in equatorially trapped, eastward propagating oscillations termed Kelvin waves. Kelvin waves in the equatorial lower stratosphere were first documented in radiosonde observations by *Wallace and Kousky* [1968]. *Salby et al.* [1984] used Limb Infrared Monitor of the Stratosphere (LIMS) temperature measurements to clearly identify equatorial Kelvin waves throughout the stratosphere and lower mesosphere (100-0.5 mb); the identification as Kelvin waves was based on (1) eastward phase progression; (2) latitudinally evanescent amplitude structure centered over the equator; and (3) vertical phase structure and propagation consistent with the Kelvin wave dispersion relation. *Hitchman and Leovy* [1988] also demonstrated good agreement between the Kelvin dispersion relation and LIMS data. LIMS also measured several trace species during its operation, namely ozone (O_3), water vapor (H_2O), nitrogen dioxide (NO_2), and nitric acid (HNO_3). This paper shows that a sizeable fraction of the tropical variance in these constituent fields also has the signature of Kelvin waves, i.e., there are equatorially trapped, eastward propagating fluctuations in all of these constituents, due to transport and temperature dependent photochemistry associated with the Kelvin waves.

Because Kelvin waves have small or zero meridional wind perturbations, tracer transport in the meridional plane occurs predominantly in the vertical direction. In the presence of a significant vertical gradient in background structure, displacements associated with Kelvin waves produce wavelike variations in conserved quantities such as potential temperature or long-lived constituent species (which act as material tracers). Kelvin waves should thus be evidenced in both temperature and tracer oscillations, and this behavior is confirmed in LIMS data here by co-locating statistically coherent temperature-tracer waves near regions of strong background gradients. The temperature fluctuations associated with Kelvin waves can furthermore influence the concentration of chemical species which are strongly temperature dependent (ozone in the upper stratosphere, for instance), and LIMS data also show evidence for this behavior. Because stratospheric Kelvin waves are observed to be sharply peaked in wave number–frequency space [e.g., *Salby et al.*, 1984], space-time spectral analysis provides a natural and powerful tool to analyze coherent fluctations in temperature and trace species. As opposed to the more complicated situation in midlatitudes where meridional advections are important [e.g., *Douglass et al.*, 1985], chemical fluctuations associated with equatorial Kelvin waves provide a simplified and idealized context to analyze the interplay of transport and photochemistry.

The purpose of this work is to document Kelvin wave fluctuations in equatorial trace constituent measurements from LIMS data, and quantify their relationships with temperature oscillations. All four trace species are analyzed because they each have varying photochemical lifetimes, which may additionally vary with height: O_3, H_2O, and HNO_3 are long-lived in the lower stratosphere and should behave as material tracers, while NO_2 and upper stratospheric O_3 have relatively short photochemical lifetimes and temperature dependent equilibrium concentrations. Temperature and constituent data from a preliminary version and the archival version of LIMS data (denoted V4 and V5, respectively) are analyzed here. The temperature signatures of Kelvin waves differ quantitatively but not qualitatively between V4 and V5 data. However, large qualitative differences in the Kelvin wave

Paper number 90JD-01244.
0148-0227/90/90JD-01244$05.00

constituent signatures are found between V4 and V5 data, demonstrating a sensitive dependence of constituent retrieval upon previously derived temperature profiles. The simplified temperature-constituent relationships detailed here for Kelvin wave motions provides a good cross check on the quality of the constituent retrievals in the tropics. Furthermore, these analyses can provide an idealized technique to study chemical parameterization schemes for use in simplified models.

The theory of linear Kelvin wave transport and photochemistry is discussed in section 2, and this theory is applied to observed ozone fluctuations in a following section. The data and spectral analysis techniques used are described in section 3. Section 4 gives a review of Kelvin wave signatures in the equatorial temperature field; included there is a comparison between temperature waves in V4 and V5 data. Section 5 documents Kelvin wave fluctuations in the separate constituent fields measured by LIMS. The observed ozone oscillations are compared with the linear theory calculations from section 2, incorporating accurate photochemical parameterizations; overall good agreement is found, although differences in detail are seen for both V4 and V5 data. Kelvin wave signatures in LIMS derived H_2O, HNO_3 and NO_2 data are also analyzed, and differences between LIMS V4 and V5 retrievals are quantified and discussed. Overall, V5 data are superior to V4 in the lower stratosphere, where transport induced oscillations are observed. V4 H_2O waves in the upper stratosphere are clearly spurrious; large differences in the results for other species, combined with the lack of ground truth data, make determination of the quality of V4 vs. V5 data in the upper stratosphere more problematic.

2. Linear Kelvin Wave Transport and Photochemistry

This section presents an analysis of linear Kelvin wave transport and photochemistry, in particular as applied to stratospheric ozone fluctuations. The analyses here follow the midlatitude calculations presented in *Hartmann and Garcia* [1979] and *Douglass et al.* [1985]. A review of the properties of equatorial Kelvin waves may be found in *Andrews et al.* [1987]. Because Kelvin waves have vanishing meridional velocity ($v' = 0$), the perturbation temperature equation linearized about the zonal mean flow is

$$\left(\frac{\partial}{\partial t} + \overline{u}\frac{\partial}{\partial x}\right) T' + w'S = 0 \qquad (1)$$

Here overbars denote zonal means and primes deviations therefrom. The log pressure vertical coordinate is $z = H\ell n(p_o/p)$, with $H = 7$ km and $p_o = 1000$ mbar, and other notation is standard [e.g., *Andrews et al.*, 1987].

$$S = \frac{1}{H}\left(\frac{2}{7}\overline{T} + \frac{\partial \overline{T}}{\partial z}\right)$$

is a background static stability parameter. Radiative damping of the temperature perturbations has been neglected, because realistic radiative time scales in the stratosphere (of order 10 days) are much longer than the Kelvin wave advective time scale $[k(\bar{u} - c)]^{-1}$ (of order 1-2 days for the waves considered here). Radiative heating due to ozone perturbations has also been neglected, because it is also likely small compared to advective effects (note the comparison of radiative-photochemical time constants in *Hartmann* [1978]). Linearized terms for these effects can be included in (1), with slight modifications to the equations below.

The perturbation ozone mixing ratio (μ') equation is

$$\left(\frac{\partial}{\partial t} + \overline{u}\frac{\partial}{\partial x}\right) \mu' + w'\overline{\mu}_z = -\Gamma\mu' - \Theta T' \qquad (2)$$

Here Γ is the photochemical relaxation frequency and Θ is the linearized ozone response to small temperature changes; these parameters are discussed more fully in the above references. $\bar{\mu}_z$ is the vertical gradient in background mixing ratio. Assuming wavelike solutions of the form $e^{ik(x-ct)}$, (1)-(2) may be solved to give the amplitude and phase of the perturbation ozone-temperature ratio (μ'/T'):

$$\left(\frac{\mu'}{T'}\right)_{amplitude} = \frac{\sqrt{X^2 + Y^2}}{(\overline{u} - c)^2 k^2 + \Gamma^2} \qquad (3a)$$

$$\left(\frac{\mu'}{T'}\right)_{phase} = tan^{-1}\left(\frac{Y}{X}\right) \qquad (3b)$$

with

$$X = [(\overline{u} - c)^2 k^2 \left(\frac{\overline{\mu}_z}{S}\right) - \Gamma\Theta]$$

$$Y = (\overline{u} - c)k[\Gamma\left(\frac{\overline{\mu}_z}{S}\right) + \Theta]$$

Note that for purely conservative transport [$\Gamma = \Theta = 0$ in (2)], in-phase T' - μ' variations are found, with amplitude proportional to $(\bar{\mu}_z/S)$ (i.e., purely advective transport maximizing in regions of largest background vertical gradient). Transport induced oscillations are anticipated where the photochemical lifetimes are long and $(\overline{\mu}_z/S)$ is large; contour plots of the latter quantity are included for the tracers in section 5. In the pure photochemical limit of very short lifetimes, i.e., $\left(\frac{\partial}{\partial t} + \overline{u}\frac{\partial}{\partial x}\right) << \Gamma$, out of phase oscillation are found, with (μ'/T') amplitude equal to $(-\Theta/\Gamma)$.

3. Data and Analyses

3.1. *LIMS Data*

LIMS temperature and trace constituent measurements are analyzed here; documentation of the LIMS experiment, along with the precision and accuracy of the various measurements, is found in *Gille and Russell* [1984] and references therein. Daily global mapped fields are derived from individual vertical profiles via the Kalman filter sequential estimation technique [*Rodgers*, 1976], and archived in the form of zonal Fourier coefficients (up to wave 6) every 4° latitude. 1-2-1 latitudinal smoothing is applied to the individual wave coefficients. Temperature and ozone data are available on the following standard pressure levels: 100, 70, 50, 30, 16, 10, 7, 5, 3, 2, 1.5, 1.0, 0.7, 0.5, 0.4, 0.2 and 0.1 mb (spacing near 3.5 km). Due to varying signal to noise ratios, retrieval pressure levels are restricted for the other constituent measurements: 70-1 mb for the H_2O data, and 70-3 mb for the HNO_3 and NO_2 data. Ascending and descending orbital data (day and night measurements, respectively) are com-

bined for all quantities except NO_2, which exhibits a large diurnal variation. Day and night NO_2 spectra are calculated separately, and cross-spectra with temperatures are calculated using the respective ascending/descending orbit temperature retrievals.

Two sets of LIMS retrievals are analyzed here. A preliminary version, denoted V4, is the same as the data analyzed in *Salby et al.* [1984] and *Hitchman and Leovy* [1986,1988]. Results using the archival version of LIMS, denoted V5, are also presented; these data are also studied in *Sun and Leovy* [1990]. The fundamental difference between the two temperature retrieval schemes are their sensitivity to short vertical scale features. Due to radiative transfer considerations, vertical wavelengths $\leq$ 10 km are inherently suppressed in limb-viewing geometry; V4 retrievals make an explicit attempt to enhance these small scales [*Bailey and Gille*, 1986]. *Hitchman and Leovy* [1986] discuss differences in tropical temperatures between V4 and V5 data; there is overall qualitative agreement, although V4 exhibits stronger variations in the vertical and agrees better with rocket profiles for rapidly varying features. For the Kelvin waves studied here, V4 data exhibit amplitudes approximately 1.5 times larger than those in V5; this V4/V5 temperature ratio is found to be about the same for Kelvin waves with vertical wavelengths of 20 and 40 km (as shown below).

Constituent profiles are calculated from the inverted temperature structure and radiances from trace species channels on LIMS. V5 inversions furthermore smooth the temperatures in the vertical prior to the constituent retrievals (E. Remsburg, personal communication, 1990). Given that the V4 and V5 temperature profiles are different, it is not unexpected that differences are found between the V4 and V5 constituent profiles. However, the vertical structures of constituent profiles associated with Kelvin waves reveal significant qualitative changes between V4 and V5, and results from both data are presented for comparison.

The LIMS instrument operated over the period 25 October, 1978 to 28 May, 1979. Kelvin wave activity shows a strong seasonal variation in the upper stratosphere, peaking during easterly regimes of the zonal wind semiannual oscillation [see *Hitchman and Leovy*, 1988]. Because we wish to analyze strong Kelvin waves throughout the entire stratosphere, we choose the 120-day segment 1 December, 1978 to 30 March, 1978 for the present analyses.

3.2. *Spectral Analyses*

Because stratospheric Kelvin waves are observed to be sharply peaked in zonal wave number-frequency space [see *Salby et al.*, 1984], space-time cross-spectral analysis is well suited for their study. Eastward-westward propagating cross-spectral power for zonal wave number k at frequency $\pm\ \omega$ (positive corresponding to westward movement) is calculated according to

$$P_{k,\pm\omega} = \frac{1}{4}[P_\omega(C_k) + P_\omega(S_k) \pm 2Q_\omega(C_k, S_k)] \qquad (4)$$

Here $P_\omega(C_k)$ is the power estimate at frequency ω for the zonal wave k cosine coefficient time series, likewise $P_\omega(S_k)$ for the sine coefficient, and $Q_\omega(C_k,S_k)$ is the quadrature spectrum estimate between C_k and S_k. Calculations here were made by direct Fourier transformation of the time series; explicit equations are given in *Hiyashi* [1971, equation 4-2]. Power spectra at frequency ω_o are smoothed in frequency using a Gaussian shaped spectral window of the form

$$W(\omega - \omega_o) = e^{-((\omega-\omega_o)/\Delta\omega)^2} \qquad (5)$$

with $\Delta\omega = 2$. Testing with several spectral resolutions has shown this choice to give a good balance between spectral resolution and stability.

Estimates of the coherence squared and phase spectra between temperature (T) and constituent (O_3, for example) time series are calculated according to

$$Coh^2_{k,\pm\omega} = \frac{K^2_{k,\pm\omega}(T,O_3) + Q^2_{k,\pm\omega}(T,O_3)}{P_{k,\pm\omega}(T)\cdot P_{k,\pm\omega}(O_3)} \qquad (6)$$

$$Ph_{k,\pm\omega} = tan^{-1}\left[\frac{Q_{k,\pm\omega}(T,O_3)}{K_{k,\pm\omega}(T,O_3)}\right] \qquad (7)$$

Here $K_{k,\pm\omega}(T,O_3)$ and $Q_{k,\pm\omega}(T,O_3)$ are the co-spectra and quadrature spectra between T and O_3 time series, with explicit formulas given in *Hiyashi* [1971, equation 4-10]. The coherence squared (6) is analogous to the squared correlation coefficient evaluated over a particular frequency band.

It is necessary to correctly estimate the number of degrees of freedom of the windowed $Coh^2_{k,\pm\omega}$ spectra to properly evaluate significant coherence levels. Here degrees of freedom (df) are estimated for the Gaussian spectral window (5) by noting that each independent Fourier harmonic in a spectral band has 2df, and then estimating the effective number of independent Fourier harmonics (n) in the spectral window of width 2N+1 according to

$$n = 2df = \frac{\left(\sum_{i=-N}^{N} P_{\omega_i}\right)^2}{\sum_{i=-N}^{N} P_{\omega_i}{}^2} \qquad (8)$$

[*Blackman and Tukey*, 1958, p. 24], where the power spectral estimates at discrete frequencies P_{ω_i} are given from (4). The limiting coherence squared at probability level p is then determined from

$$\beta = 1 - p^{[1/(\frac{df}{2}-1)]} \qquad (9)$$

as in *Julian* [1975].

Coherence squared calculations are made using the Gaussian window (5), with $\Delta\omega = 4$ (the window is wider than that used for the power spectra to give greater statistical stability). n was calculated from (8), giving values of order 6 for the spectra here. 90%, 95% and 99% confidence levels for the coherence squared are calculated from (9), giving values near .369, .451 and .602, respectively. Contour plots of $Coh^2_{k,\pm\omega}$ (hereafter referred to as simply coherence) are drawn such that only regions above the 90, 95 and 99% confidence levels are shown, with regions above the 95% level stippled.

4. Kelvin Wave Temperature Signatures

Temperature signatures of Kelvin waves in the LIMS V4 data were reported by *Salby et al.* [1984]. A

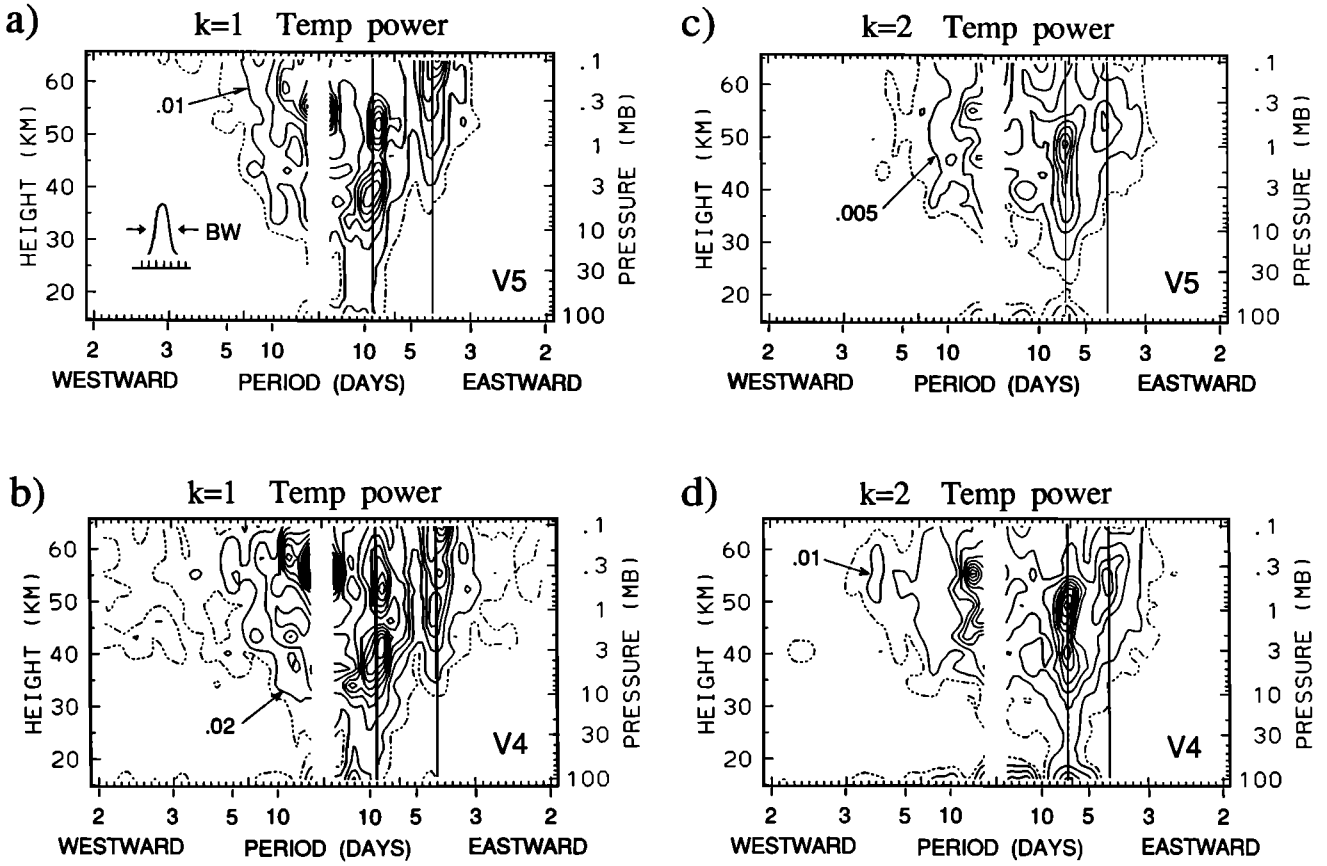

Fig. 1. Height-frequency sections at the equator of zonal wave 1 (left) and 2 (right) temperature spectral power density from LIMS V5 (top) and V4 (bottom) data. Units are $K^2 \cdot \Delta\omega^{-1}$, with $\Delta\omega$ the unit frequency interval of $(2\pi/120$ days). The spectral bandwidth (BW) is indicated in the upper left panel. Contour intervals (solid lines) are noted in each panel, and dashed lines are one half the lowest contour level. Note the V4 contour intervals are double those for V5. Vertical lines in these and the following figures denote the location of spectral maxima associated with Kelvin waves.

review of the temperature waves is shown here to provide background for the constituent oscillations. Additionally, V4 and V5 temperature data are compared.

Figure 1 shows height-frequency sections at the equator of eastward-westward spectral power density for zonal waves 1 and 2, from LIMS V4 and V5. Strong maxima are seen corresponding to eastward moving waves with periods near 8.6 and 4 days for wave 1 (Figures 1a and 1b), and 6.3 and 4 days for wave 2 (Figures 1c and 1d), in both versions of the data. Overall the spectra are very similar, with the exception that V4 has approximately 2-3 times the spectral power of V5 (note that wave amplitudes are proportional to the square root of the power, so that Kelvin wave amplitudes are 1.4-1.7 times larger in V4 data).

Figure 2 shows a meridional cross section of the amplitude and phase of the eastward moving wave 1 feature centered near periods of 8.6 days, from V4 data. Wave amplitude is calculated as the square root of twice the power (4), integrated over a frequency band centered at a period of 8.6 days. Notable features of the Kelvin wave shown in Figure 2 are (1) amplitude maxima centered near the equator, with an evanescent decrease in amplitude away from the equator; (2) in phase horizontal structure; (3) eastward phase tilt with height (denoting downward phase progression for this eastward

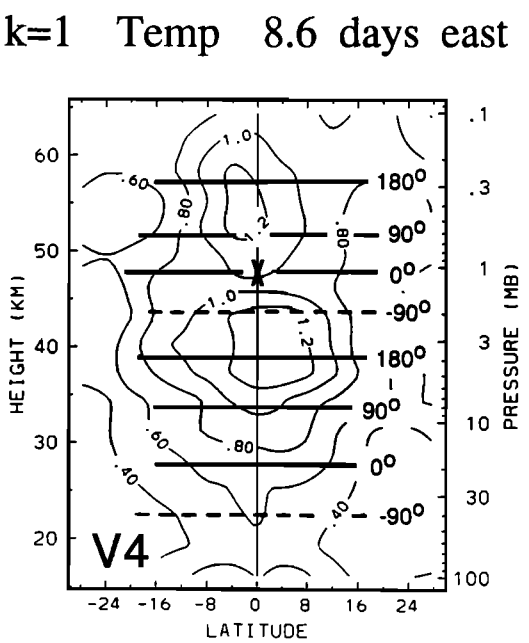

Fig. 2. Meridional cross section of amplitude (contour interval of 0.2 K) and phase (in degrees, with respect to the 1 mb level at the equator) of the zonal wave 1, 8.6 day eastward moving temperature wave in V4 data.

propagating wave), with a vertical wavelength of order 18 km. Overall similar wave structure is found using V5 data, with the exception that the amplitude is reduced by a factor of approximately 1.5. This V4/V5 amplitude ratio is similarly found for the 4.0 day wave 1 feature (Figures 1a and 1b), which has a vertical wavelength near 40 km.

5. KELVIN WAVE-INDUCED CONSTITUENT OSCILLATIONS

5.1. *Ozone Observations*

Figure 3 shows height-frequency ozone power spectra at the equator for zonal waves 1 and 2, from LIMS V5 and V4 data. Each of these spectra shows peaks corresponding to eastward moving waves at the frequencies identified in the temperature spectra (Figure 1). *Sun and Leovy* [1990] also noted the eastward travelling ozone waves in the LIMS V5 data. There is, however, a considerable degree of difference in the details of the spectra in Figure 3. LIMS V5 and V4 show quite distinct vertical structures: V4 power peaks over 3-10 mb, whereas V5 maximizes near 30 mb.

Figure 4 shows meridional cross sections of the amplitude and phase of eastward moving zonal wave 1 in ozone centered near periods of 8.6 days, for LIMS V5 and V4 data. Both data show amplitude maxima centered on the equator, in phase horizontal structure, and eastward phase tilt with height in the upper stratosphere with a wavelength near 18 km (cf. Figure 2). V5 data show amplitude maxima near 3 mb, 30 mb and below 70 mb, while V4 data have a single maximum near 5 mb. V5 data exhibit eastward phase tilt with height in the lower to middle stratosphere, whereas V4 shows little phase variation with height below the amplitude maximum near 5 mb.

Spectral coherence between zonal wave 1 coefficients in temperature and ozone (T - O_3) is shown as functions of height and frequency in Figure 5 for LIMS V5 and V4. Stippled regions represent coherency above the 95% confidence level, as discussed in section 3.3, i.e., these denote vertical levels and frequencies for which the temperature and ozone waves are significantly correlated. Significant coherence is found in the upper stratosphere (40-55 km) for the eastward moving 8.6 and 4.0 day features, along with low frequency westward moving waves in both V5 and V4. These latter features are likely associated with planetary wave incursions from the NH winter stratosphere. The coherence patterns are somewhat different between V4 and V5 data in the lower stratosphere, with V5 showing coherence over a deeper vertical region for the 8.6 day Kelvin wave.

Figures 6a and 6b show meridional cross sections of the T-O_3 coherence for the eastward moving 8.6 day wave 1 feature, calculated from V5 and V4 data. These are calculated by integrating the appropriate quantities

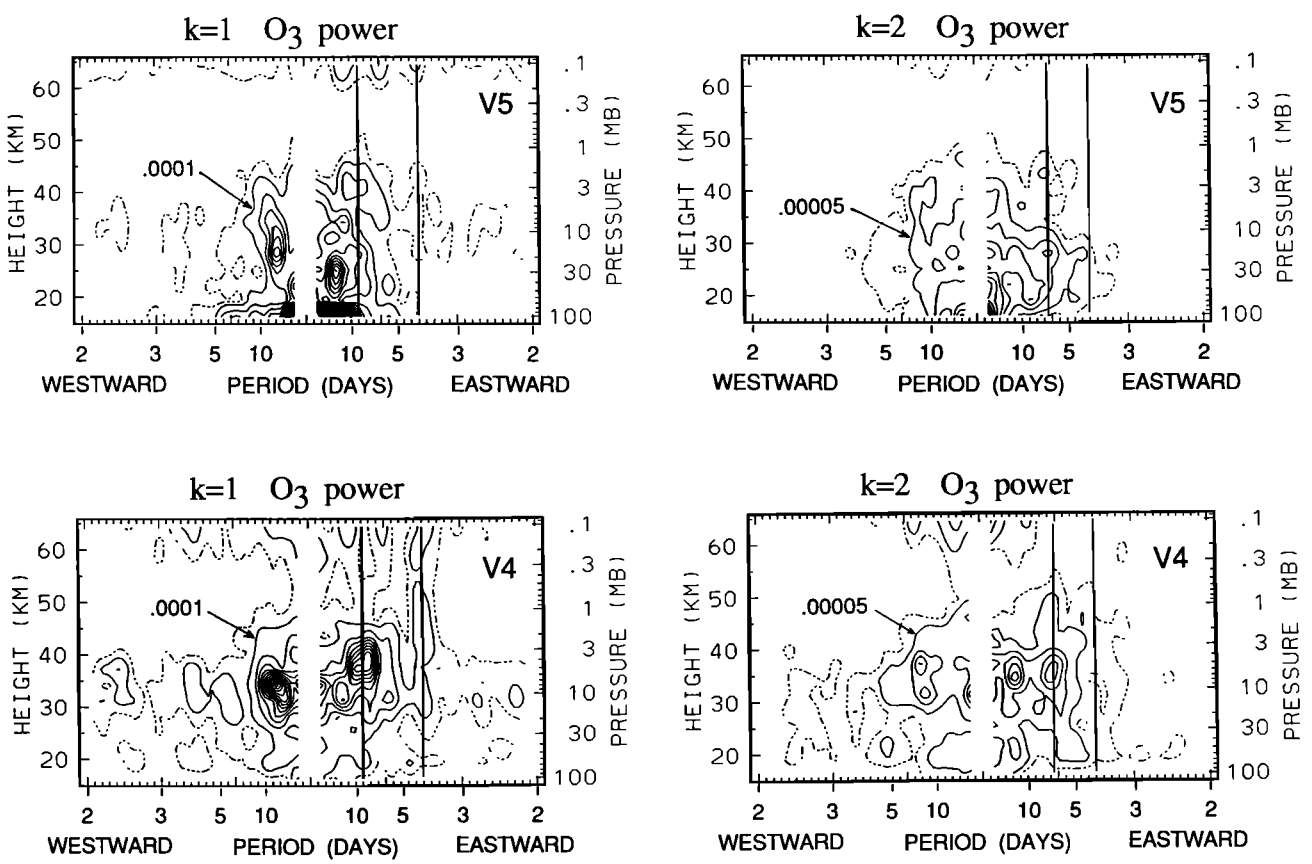

Fig. 3. Height-frequency cross sections at the equator of zonal wave 1 (left) and 2 (right) ozone power spectral density, from LIMS V5 (top) and LIMS V4 (bottom) data. Units are ppmv^2 · $\Delta\omega^{-1}$. Contour interval (solid lines) are noted in each panel, and dashed lines are one half the lowest contour interval.

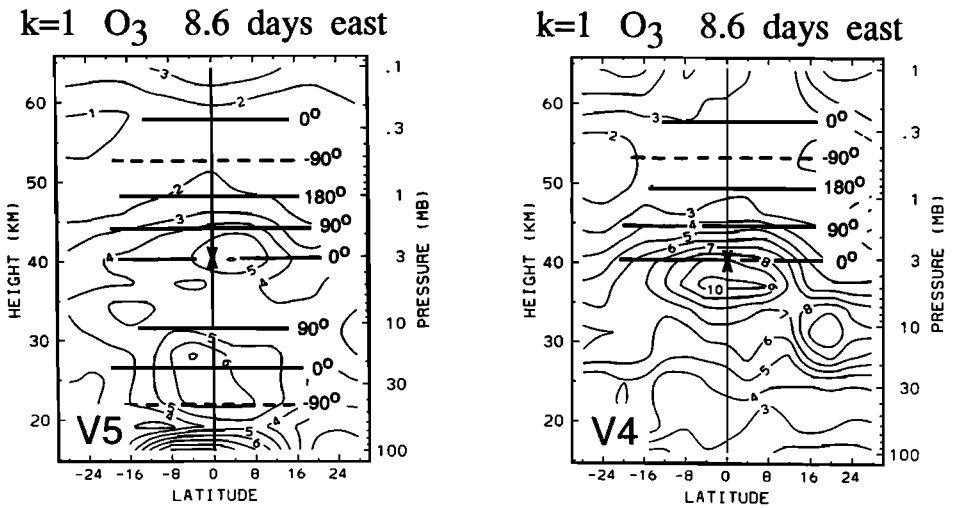

Fig. 4. Meridional cross sections of the amplitude (contour interval of 0.01 ppmv) and phase (in degrees, with respect to the 3 mb level at the equator) of zonal wave 1, 8.6 day eastward moving ozone oscillations in LIMS V5 (left) and V4 (right) data.

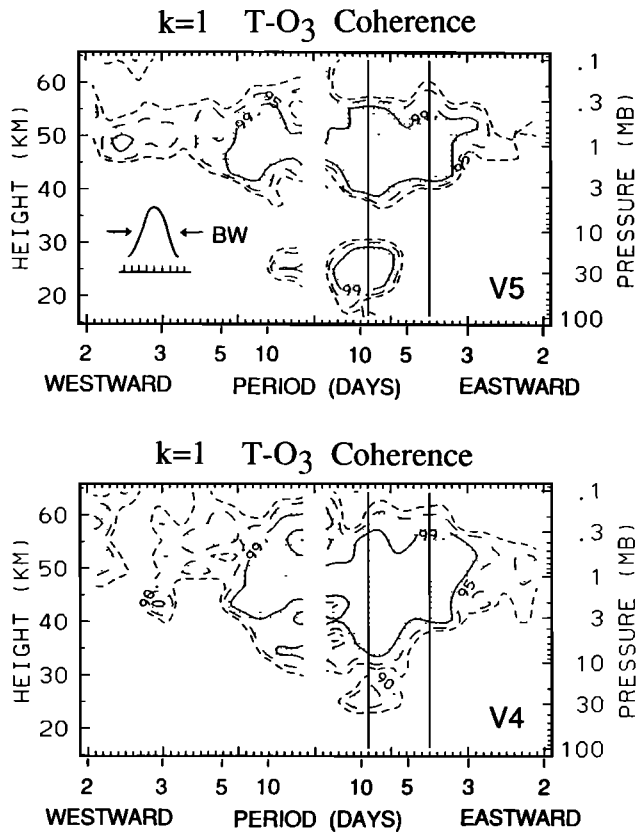

Fig. 5. Height-frequency sections of wave 1 $T\text{-}O_3$ coherence for LIMS V5 (top) and V4 (bottom) data. Contours represent coherence values significant above the 90 (short dashed), 95 (long dashed) and 99% (solid lines) confidence levels, as discussed in section 3.3. Values above the 95% level are shaded. The spectral bandwidth (BW) is also indicated.

over a frequency band centered at a period of 8.6 days. Each section shows two separated regions of significant coherence: one in the upper stratosphere and one in the lower stratosphere. LIMS V5 shows a broader and deeper area of coherence in the lower stratosphere than that in V4. Quantitative differences in these two data sets is discussed following the comparison with the linear model below (where Figure 6c is also discussed).

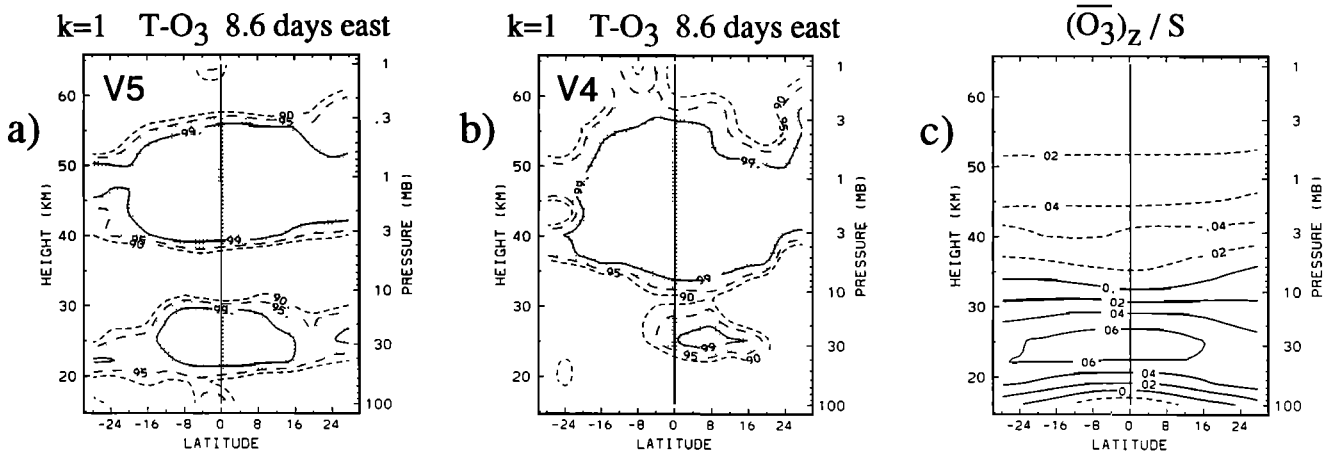

Fig. 6. Meridional cross sections of T-O_3 coherence for the zonal wave 1, 8.6 day eastward moving Kelvin wave, for (a) LIMS V5 and (b) V4 data. Contours as in Figure 5. (c) Meridional section of $(\bar{\mu}_z/S)$ for ozone, with contour interval of 0.02 ppmv/K. This quantity is important for Kelvin wave transport, as described in section 2.

5.2. *Comparison with Linear Theory*

In this section the observed T-O_3 data is compared to results from the linear model equations of section 2. In particular, we compare the amplitude and phase of coherent T-O_3 waves between model and data. Equations (3a) and (3b) give the model amplitude and phase. Γ and Θ model parameter values used here are obtained from a parameterization scheme described in *Stolarski and Douglass* [1985]; these were provided by A. Douglass (private communication, 1989) and shown in Figure 7. A second, independent set of parameter values are also used and shown in Figure 7; these were obtained from a two-dimensional coupled chemical-dynamical-radiative model [*Brasseur et al.*, 1990], as provided by A. Smith (private communication, 1989). The quantity $(\bar{\mu}_z/S)$ is calculated from 120-day mean $\bar{\mu}$ and $\bar{T}$ fields from LIMS data, and is shown in Figure 6c, and 120-day mean $\bar{u}$ based on LIMS data is used.

Data-model comparisons are made for two observed Kelvin modes (cf. Figures 1-3): wave 1, 8.6 day period ($c = 54$ ms^{-1}), and wave 2, 6.3 day period ($c = 37$ ms^{-1}). Observed T-O_3 phase difference is calculated from (7). Observed (μ'/T') amplitudes are calculated for the spectral bands studied here via

$$a = \left[\frac{K^2_{k,\pm\omega}(T, O_3) + Q^2_{k,\pm\omega}(T, O_3)}{P^2_{k,\pm\omega}(T)} \right]^{1/2} \qquad (10)$$

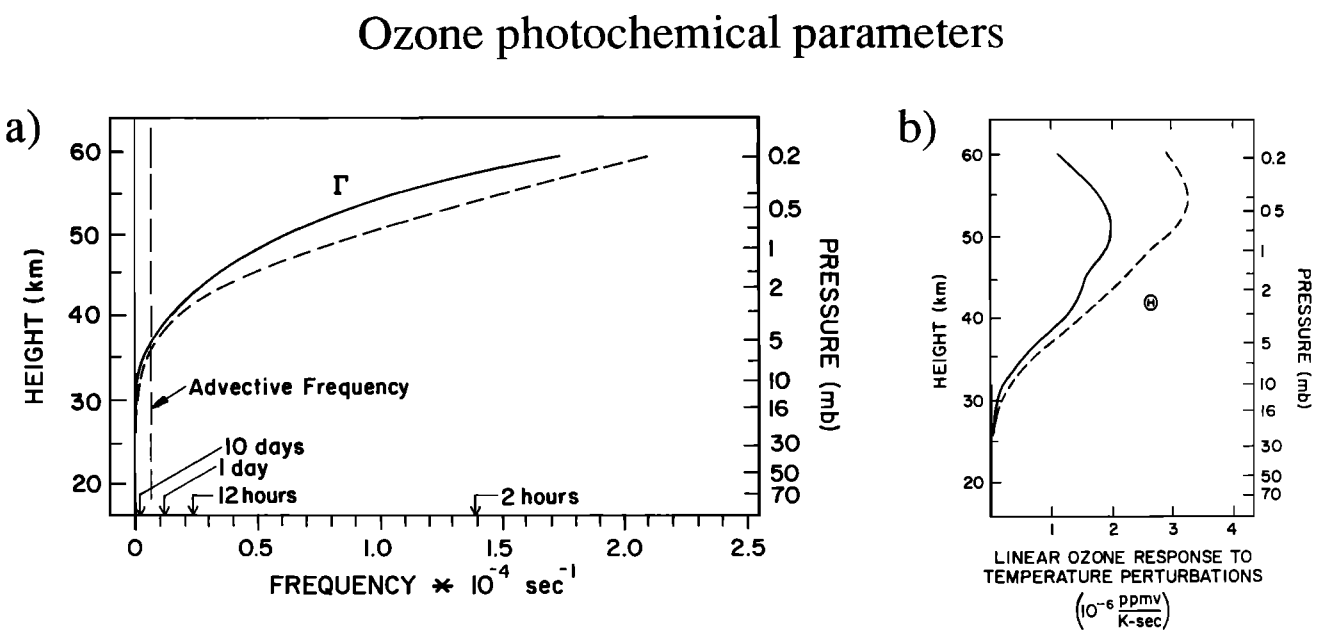

Fig. 7. (a) Γ parameter values used in equations (2) and (3), obtained from *Stolarski and Douglass* [1985] (dashed lines) and from the model of *Brasseur et al.* [1990] (solid lines). Also shown is the advective frequency for zonal wave 1 Kelvin wave with a 10-day period. (b) Θ parameters, from the same references as in Figure 7a.

This equation is equivalent to linear regression over the associated frequency band. It is also equivalent to the product of T-O_3 coherence squared (6) with $(P(O_3)/P(T))^{1/2}$; this latter quantity is proportional to the ozone-temperature amplitude ratio, which can be compared for the wave 1 mode in Figures 2 and 4.

Figure 8 shows the T-O_3 amplitude and phase for both Kelvin wave modes from LIMS V4 and V5 data, together with model results using both sets of parameter values. Model results incorporating the two sets of parameters are very similar. Both model and observations in Figure 8 exhibit the same overall character of out of phase variations in the upper stratosphere (above 35 km) and in phase waves below. There are, however, considerable differences in detail in the (μ'/T') amplitude ratios in Figure 8. In the uppermost levels above 2 mb, model and observed ratios are in good agreement. Over 10-3 mb, V4 ratios are larger than both V5 and model results; furthermore, the wave 2 V4 profile is the only one that does not exhibit the characteristic (μ'/T') ratio minimum in the transition region near 10 mb.

Transport is the dominant mechanism for T-O_3 coherence in the lower stratosphere. Here the ratio $(\bar{\mu}_z/S)$, as measured by LIMS, gives a firm estimate of the (μ'/T') ratio. LIMS V5 shows nearly exact in phase T-O_3 behavior below 10 mb for both modes, but the (μ'/T') amplitude is a factor of 2-3 too large (Figure 8). LIMS V4 show too small (μ'/T') amplitude (note the waves are not coherent below 30 mb in V4 data, Figure 6a), and the measured T-O_3 phase difference is not close to zero. V4 and V5 data thus apparently both have problems in the lower stratosphere, although the overall transport signatures of statistically significant coherence and in phase behavior are more accurately captured in V5 data.

5.3. *Water Vapor*

Figure 9 shows height-frequency sections of wave 1 H_2O spectral power from V4 and V5 data. V4 shows maxima for eastward Kelvin wave periods, whereas V5 gives only a hint of such peaks. Figure 10 shows cross sections of

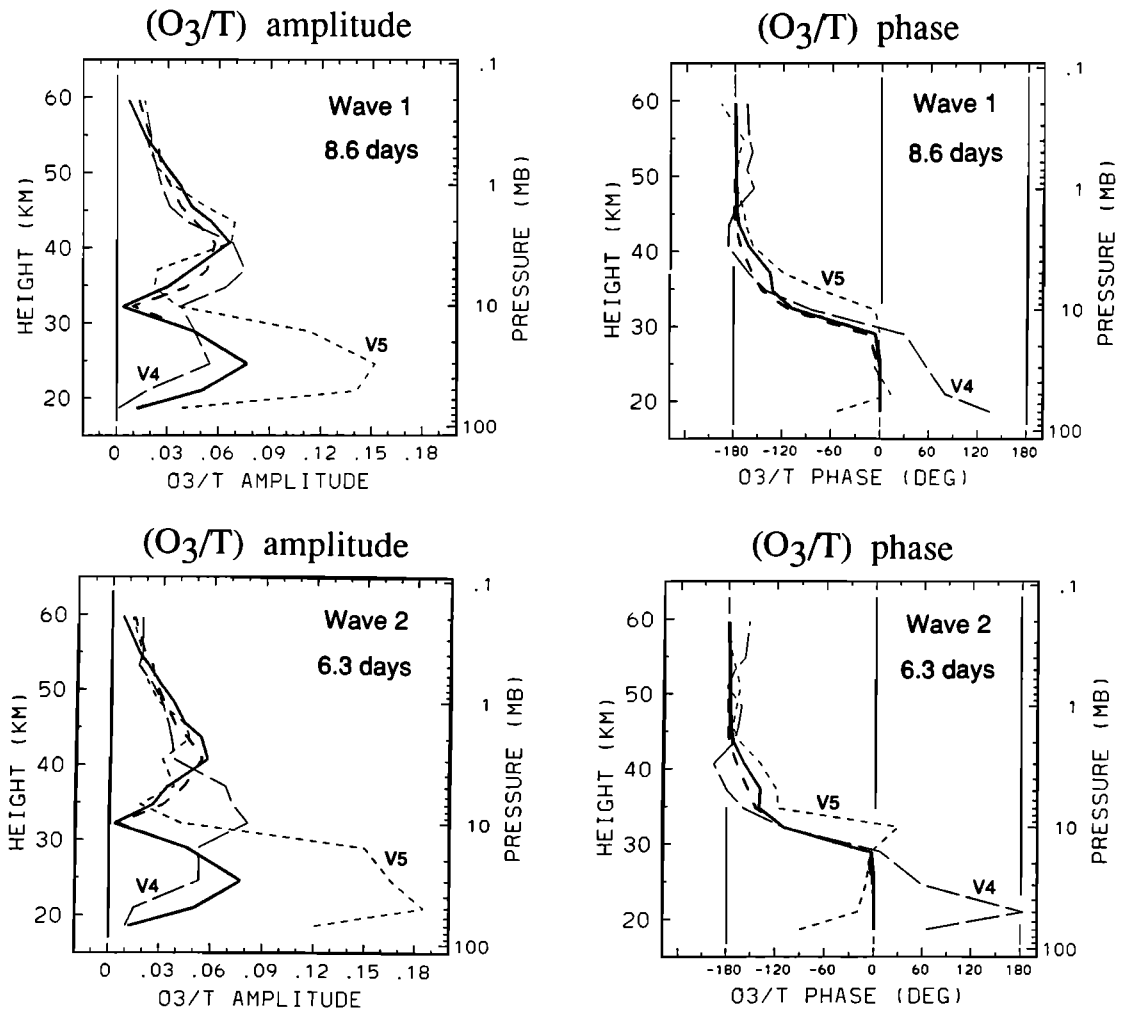

Fig. 8. Left panels show (μ'/T') amplitude for T-O_3 waves calculated from the model of section 2 using equation (3a), and from LIMS V4 and V5 data via (10). Heavy solid and dashed lines are model results based on the solid and dashed parameter values shown in Figure 7. Right panels show T-O_3 phase difference at the equator for the model (3b) and observations (7). Negative phase denotes temperature waves lead ozone waves in time. Top figures are for zonal wave 1 with 8.6 day period, and lower figures for wave 2, 6.3 day period.

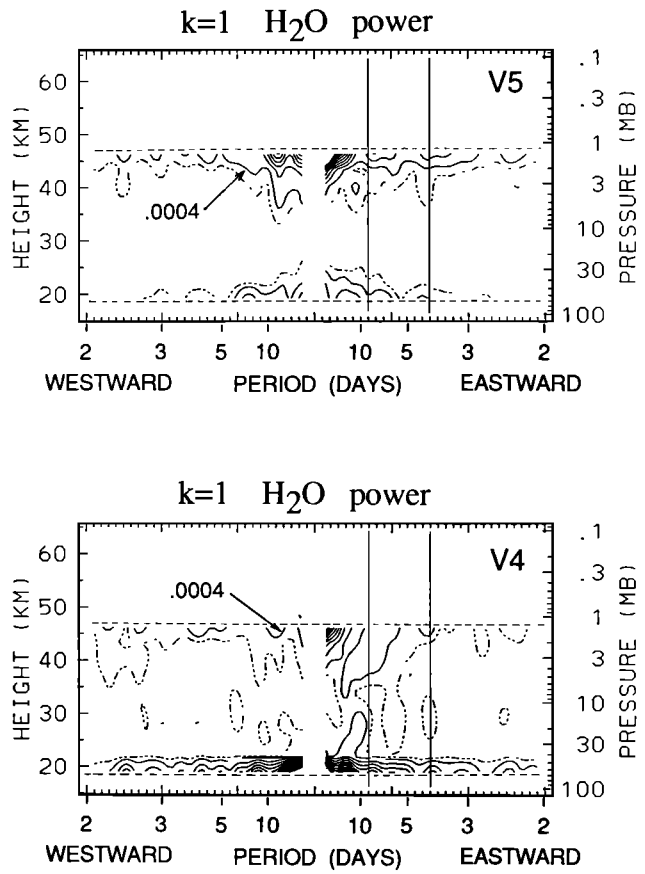

Fig. 9. Height-frequency sections of zonal wave 1 H_2O spectral power density for LIMS V5 (top) and V4 (bottom) data. Units are ppmv$^2 \cdot \Delta\omega^{-1}$. Contours as in Figure 1.

T-H_2O coherence for the 8.6 day wave 1 feature from both V4 and V5, along with the T-H_2O phase difference tabulated at each level where the coherence is significant. These figures reveal the most dramatic differences seen between V4 and V5 in the constituent fields. V4 shows strong coherence over much of the region analyzed, and the T-H_2O oscillations are out of phase. V5 shows a small region of in phase coherence centered near 50 mb, with a hint of in phase behavior near 2 mb. Both of these latter regions show relative positive maxima in $(\bar{\mu}_z/S)$ (Figure 10c), and the V5 data are thus consistent with transport induced H_2O waves. However, the calculated (μ'/T') ratios in these regions from V5 are in the range 0.05-0.15 ppmv/K, 3-10 times larger than $(\bar{\mu}_z/S)$ for H_2O in Figure 10c, and hence not in quantitative agreement with transport (recall that V5 data also shows too large (μ'/T') for ozone transport, e.g., Figure 8).

The out of phase T-H_2O behavior seen in V4 (Figure 10b) is inconsistent with transport. Furthermore, because the photochemical lifetime of H_2O is of the order of several months below 60 km [*Brasseur and Solomon*, 1984, Figure 5.21], there should be little temperature dependent photochemical variation in H_2O. Hence the patterns seen in V4 are likely not true H_2O waves, but possibly reflect an artificial dependence on temperature in the retrieval process.

5.4. *Nitric Acid*

Figure 11 shows height-frequency cross sections of zonal wave 1 HNO_3 spectral power for V4 and V5 data. V4 shows a clear peak for the eastward 8.6 day feature over 10-3 mb; V5 also shows a maximum in this region, reduced in amplitude compared to V4. Both spectra in Figure 11 show a strong spectral peak at 16 mb corresponding to a westward moving wave near 15 day period; latitude-frequency sections (not shown) reveal this equatorial peak to be connected with northern and southern hemisphere midlatitude maxima. Similarly positioned westward spectral maxima are seen in O_3 near 10 mb (Figure 3). Although the nature (and statistical significance) of this feature is unclear, *Madden and Labitzke* [1981] have documented a strong westward moving wave 1 disturbance of similar period in the NH stratosphere and troposphere during part of the period of observation here (January 1979), noting characteristics similar to that expected of global Rossby normal mode oscillations. Note however that this HNO_3 feature is not coherent with temperature in either V4 or V5 data (not shown here).

Figure 12 shows meridional cross sections of T-HNO_3 coherence and tabulated phase for the 8.6 day wave 1 feature, from V4 and V5. V4 shows out of phase T-

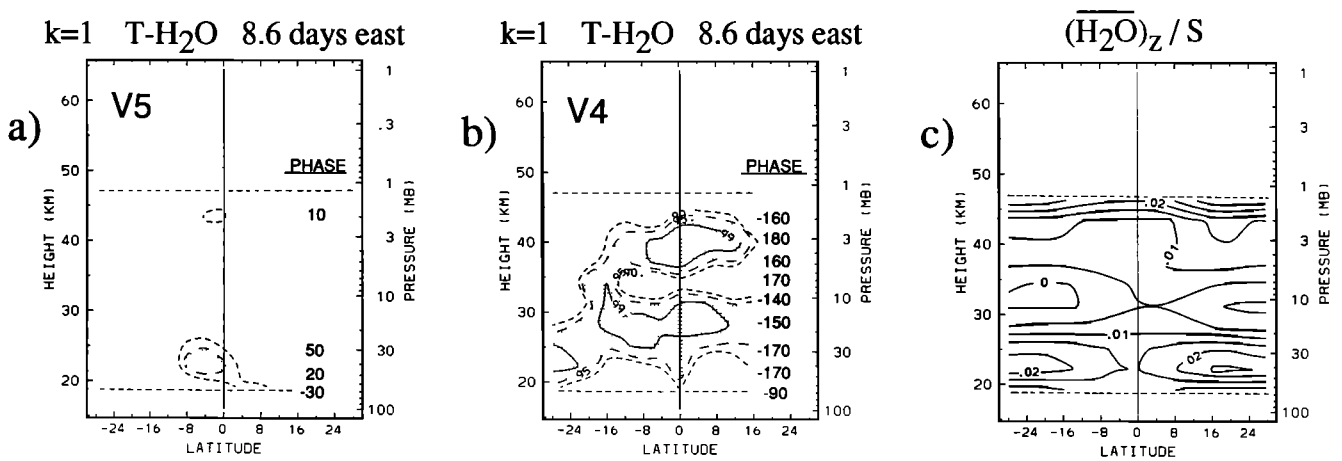

Fig. 10. Meridional cross sections of T-H_2O coherence for zonal wave 1, 8.6 day Kelvin waves, from (a) LIMS V5 and (b) V4 data. Contours as in Figure 5. Also added are T-H_2O phase differences (in degrees) at the equator. (c) $(\bar{\mu}_z/S)$ for H_2O, with contour interval of 0.005 ppmv/K.

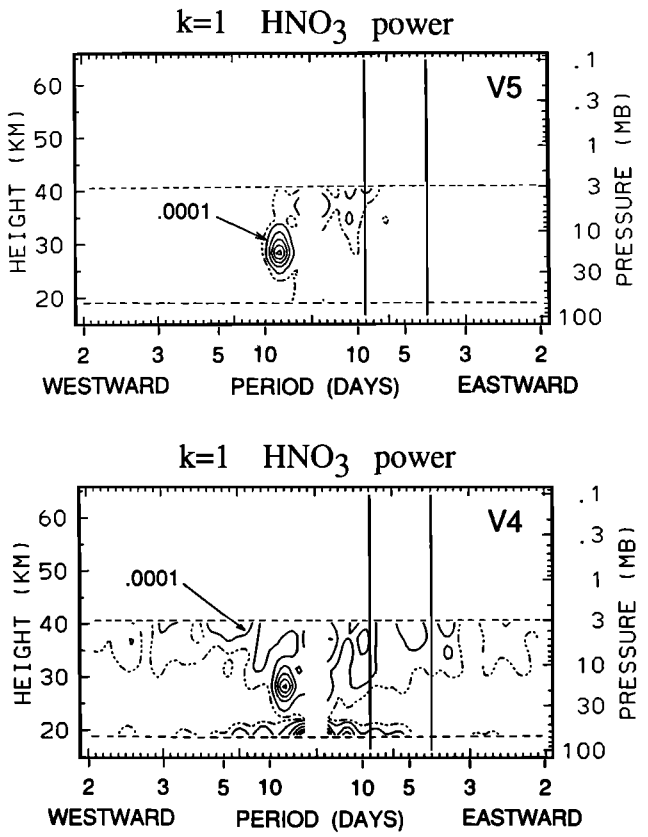

Fig. 11. Height-frequency cross sections of wave 1 HNO_3 spectral power density for LIMS V5 (top) and V4 (bottom) data. Units are ppbv$^2 \cdot \Delta\omega^{-1}$. Contours as in Figure 1.

HNO_3 waves over 10-3 mb. V5 shows nearly in phase oscillations in the lower stratosphere (70-16 mb), with a hint of out of phase behavior at the 3 mb level. The photochemical lifetime of HNO_3 is long compared to the Kelvin wave advective time (1-2 days) below 30 km [*Brasseur and Solomon*, 1984, Figure 5.38], and nitric acid thus should behave as a tracer there. The in phase oscillations seen in V5 (Figure 12a) are consistent with transport in the lower stratosphere; note the relative positive maximum in $(\bar{\mu}_z/S)$ in this region in Figure 12c. As with O_3 and H_2O, the (μ'/T') ratio from V5 is somewhat larger than the calculated $(\bar{\mu}_z/S)$. HNO_3 has a short photochemical lifetime in the upper stratosphere, and the out of phase signatures seen in Figures 12a and 12b may be evidence of temperature dependent equilibrium concentrations. However, in light of (1) the different patterns found for V4 and V5 data in Figure 12; (2) clear errors in the upper stratospheric V4 H_2O data (Figure 10b and discussion above); and (3) lack of ground truth or model for comparison, the out-of-phase patterns in Figures 12a and 12b may only show the sensitivity of HNO_3 retrieval scheme to the temperature profile.

5.5. *Nitrogen Dioxide*

NO_2 exhibits a large diurnal variation in the upper stratosphere because of fast photolytic conversion to NO which occurs in sunlight; nighttime zonal mean values at 40 km are of order 4 times as large as daytime values [*Brasseur and Solomon*, 1984]. Because of this variability, daytime and nighttime NO_2 variations are analyzed separately here, based on retrievals processed from the independent ascending and descending satellite orbital measurements, respectively (see section 3.1). Figure 13 shows height-frequency sections of zonal wave 1 spectral power for day and night NO_2 variations, for both LIMS V4 and V5. All the cross sections show power maxima for the 8.6 day feature at and above 10 mb. Nighttime wave power is an order of magnitude larger than daytime in both data sets, consistent with the large zonal mean variations discussed above. V4 power is of the same order as V5 in daytime, and 5-10 times larger at night.

Figure 14 shows height-frequency sections of wave 1 T-NO_2 coherence. V4 data exhibits strong coherence over the entire region of analysis for both day and night waves; V5 shows coherence only over 10-5 mb. All of the T-NO_2 coherent fluctuations in Figure 14 are out of phase, except the daytime V5 which are in phase. Out of phase variations are consistent with the short photochemical lifetime of NO_2 throughout the stratosphere [*Brasseur and Solomon*, 1984, Figure 5.38]; the in phase waves seen in daytime V5 are questionable because this is near a zero of $(\bar{\mu}_z/S)$ (not shown), and hence not due to transport. Overall the large differences in NO_2 power

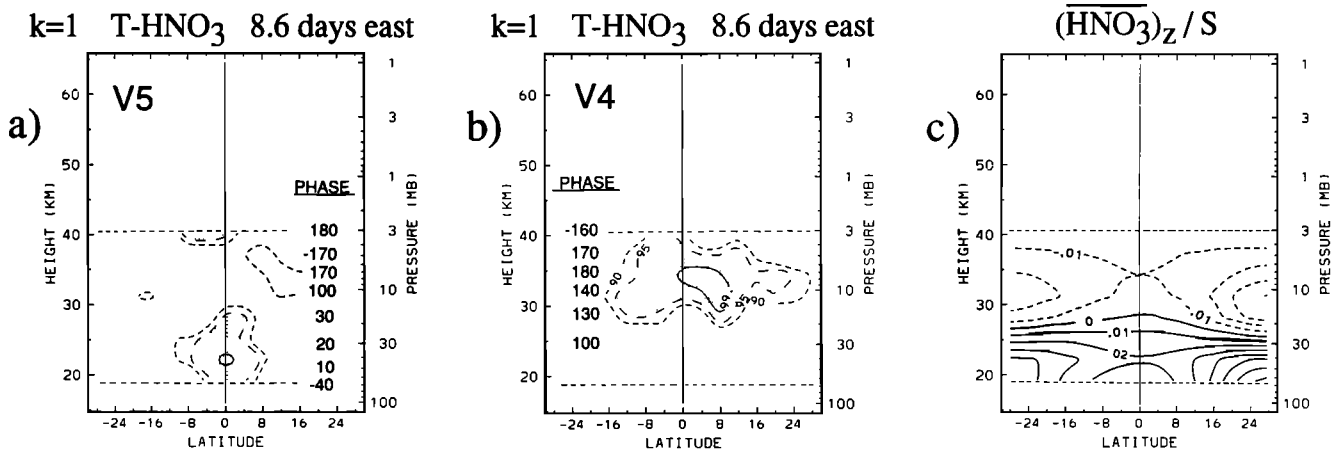

Fig. 12. Meridional cross sections of T-HNO_3 coherence for zonal wave 1, 8.6 day Kelvin waves, from (a) LIMS V5 and (b) V4 data. Contours as in Figure 5. Also added are T-HNO_3 phase differences (in degrees) at the equator. (c) $(\bar{\mu}_z/S)$ for HNO_3, with contour interval of 0.01 ppbv/K.

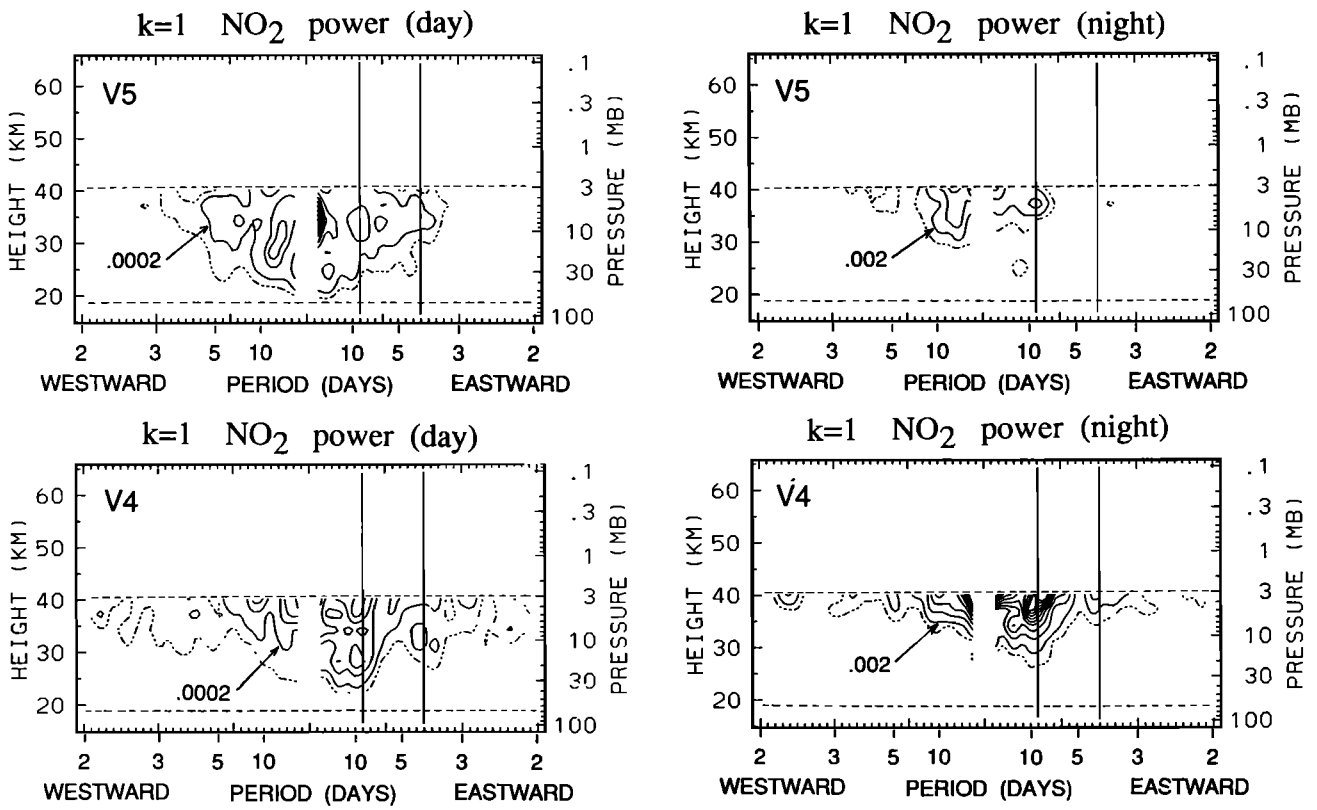

Fig. 13. Height-frequency sections of wave 1 NO_2 power spectral density during day (left) and night (right), from LIMS V5 (top) and V4 (bottom) data. Units are $ppbv^2 \cdot \Delta\omega^{-1}$. Contours as in Figure 1. Note the contour intervals are the same for V4 and V5 data, but change by an order of magnitude between day and night.

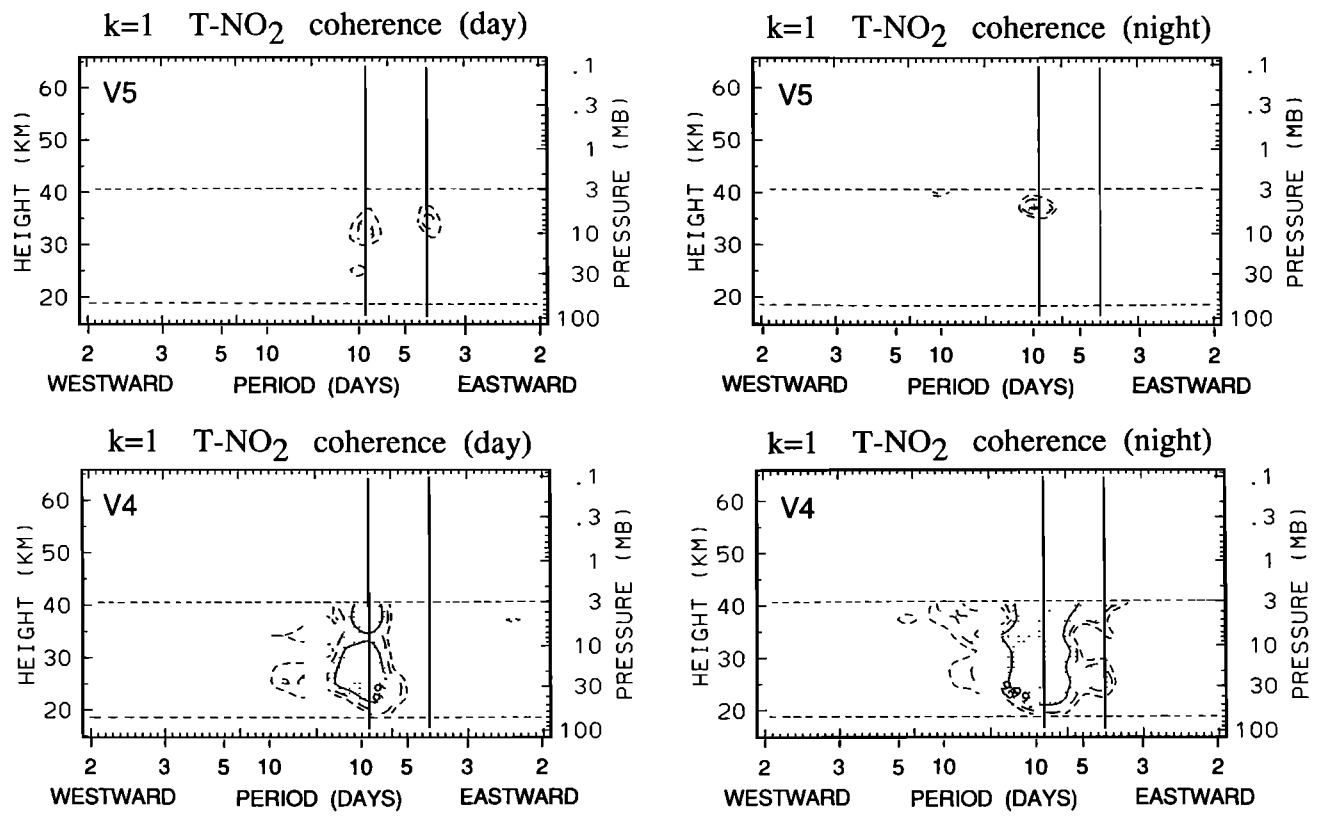

Fig. 14. Height-frequency sections of wave 1 $T\text{-}NO_2$ coherence for day (left) and night (right) measurements, from LIMS V5 (top) and V4 (bottom) data. Contours as in Figure 5.

and coherence spectra between V4 and V5 data do not promote confidence in the Kelvin wave results of either retrieval.

6. Summary and Discussion

Kelvin waves are a ubiquitous feature of the tropical stratosphere, containing a large fraction of the space-time variance in the temperature and zonal wind fields. This study has documented Kelvin-wave induced oscillations in the constituent fields measured by the LIMS experiment. There are two clear advantages to analyzing coherent fluctations associated with Kelvin waves: (1) Kelvin waves have vanishing meridional velocity and thereby simplified transport, and (2) Kelvin waves in the middle atmosphere are sharply peaked in zonal wave number–frequency space, allowing powerful use of space-time spectral analyses for analyzing coherent phenomenon. Trace species which are long lived with respect to the Kelvin wave advective time scale, and have a significant background vertical gradient, exhibit Kelvin wave tracer oscillations. These are evidenced by strong in phase temperature-tracer coherency co-located with the region of background vertical gradient ($\overline{\mu}_z/S$); this is observed in LIMS data for lower stratospheric O_3, H_2O and HNO_3. For constituents with short photochemical lifetimes and temperature dependent equilibrium concentrations, temperature perturbations associated with Kelvin waves produce wavelike constituent fluctuations. A good example is ozone in the upper stratosphere; LIMS data show clear out-of-phase T-O_3 behavior signifying photochemical control. Analyses of Kelvin wave constituent fluctuations with methods similar to those used here may provide a method to test parameterization schemes used in simplified chemical models. Additionally, future satellite measurements of other chemical families may benefit from similar studies.

An important aspect of this study is the difference in constituent waves between LIMS V4 and V5 data. As noted in section 3.1, the retrieval of constituent fields depends on previously derived temperature information. Although Kelvin wave temperatures differ quantitatively between V4 and V5 data, fundamental qualitative differences in constituent data are found, demonstrating how sensitive the retrieval process can be. V5 data are superior to V4 in the lower stratosphere for analyzing tracer oscillations in O_3, H_2O and HNO_3 (as evidenced by in-phase T-tracer coherence in Figures 8, 10 and 12). However derived (μ'/T') ratios from V5 for all these tracers are 2-5 times as large as theoretical predicted values of ($\overline{\mu}_z/S$). This might be related to the additional smoothing applied to the V5 temperature data prior to the constituent retrieval calculations, as discussed in section 3.1. Little can be said of the relative merit of V4 and V5 ozone data in the upper stratosphere. Kelvin wave T-O_3 results from both data show overall agreement with the parameterized linear model results (Figure 8), although there are differences in detail for each. V4 H_2O waves in the middle and upper stratosphere are clearly unrealistic (Figure 10b), likely reflecting an artificial dependence on temperature in the retrieval process. V4 and V5 NO_2 results are very different, but there is no ground truth data to say which is better. It is possible that a coupled, iterative scheme for analyzing temperature and constituent profiles could avoid some of the problems uncovered here (P. Bailey, personal communication, 1990). In any case, Kelvin wave signatures provide a powerful tool to check the quality of constituent retrievals in the tropics.

Acknowledgments. The author acknowledges Paul Bailey, Guy Brasseur, Anne Douglass, Eric Fetzer, Rolando Garcia, John Gille, Roland Madden, Ellis Remsburg and Anne Smith for helpful discussions and comments. Anne Douglass and Anne Smith provided the ozone photochemical parameter values for use in the linear model. Conway Leovy, Mark Schoeberl and an anonymous reviewer provided helpful comments which significantly improved the presentation of these results. John Gille initially suggested the analysis of equatorial variations in LIMS ozone data. This work has been supported by NASA grant W16215. The National Center for Atmospheric Research is sponsored by the National Science Foundation.

References

Andrews, D. G., J. R. Holton, and C. B. Leovy, *Middle Atmosphere Dynamics*, 489 pp., Academic, San Diego, Calif., 1987.

Bailey, P. L. and J. C. Gille, Inversion of limb radiance measurements: An operational algorithm, *J. Geophys. Res., 91*, 2757-2774, 1986.

Blackman, R. B. and J. W. Tukey, *The Measurement of Power Spectra*, 190 pp., Dover, New York, 1958.

Brasseur, G. and S. Solomon, *Aeronomy of the Middle Atmosphere*, 452 pp., D. Reidel, Hingham, Mass., 1984.

Brasseur, G., M. H. Hitchman, S. Walters, M. Dymek, E. Falise, and M. Pirre, An interactive chemical dynamical radiative two-dimensional model of the middle atmosphere, *J. Geophys. Res., 95*, 5639-5655, 1990.

Douglass, A. R., R. B. Rood, and R. S. Stolarski, Interpretation of ozone temperature correlations, 2. Analysis of SBUV ozone data. *J. Geophys. Res., 90*, 10,693-10,708, 1985.

Gille, J. C. and J. M. Russell III, The limb infrared monitor of the stratosphere: Experiment description, performance, and results, *J. Geophys. Res., 89*, 5125-5140, 1984.

Hartmann, D. L., A note concerning the effect of varying extinction on radiative-photochemical relaxation, *J. Atmos. Sci., 35*, 1125-1130, 1978.

Hartmann, D. L. and R. R. Garcia, A mechanistic model of ozone transport by planetary waves in the stratosphere, *J. Atmos. Sci., 36*, 350-364, 1979.

Hitchman, M. H. and C. B. Leovy, Evolution of the zonal mean state in the equatorial middle atmosphere during October 1978-May 1979, *J. Atmos. Sci., 43*, 3159-3176, 1986.

Hitchman, M. H. and C. B. Leovy, Estimation of the Kelvin wave contribution to the semiannual oscillation, *J. Atmos. Sci., 45*, 1462-1475, 1988.

Hiyashi, Y., A generalized method of resolving disturbances into progressive and retrogressive waves by space Fourier and time cross-spectral analyses, *J. Meteorol. Soc. Jpn., 49*, 125-128, 1971.

Julian, P. R., Comments on the determination of significance levels of the coherence statistic, *J. Atmos. Sci., 32*, 836-837, 1975.

Madden, R. A. and K. Labitzke, A free Rossby wave in the troposphere and stratosphere during January 1979, *J. Geophys. Res., 86*, 1247-1254, 1981.

Rodgers, C. D., Retrieval of atmospheric temperature and composition from remote measurements of thermal radiation, *Rev. Geophys., 14*, 609-624, 1976.

Salby, M. L., D. L. Hartmann, P. L. Bailey, and J. C. Gille, Evidence for equatorial Kelvin modes in Nimbus-7 LIMS, *J. Atmos. Sci., 41*, 220-235, 1984.

Stolarski, R. S. and A. R. Douglass, Parameterization of the photochemistry of stratospheric ozone including catalytic loss processes, *J. Geophys. Res., 90*, 10,709-10,718, 1985.

Sun, C. R. and C. B. Leovy, Ozone variability in the equatorial middle atmosphere. *J. Geophys. Res., 95*, 13,829-13,849, 1990.

Wallace, J. M. and V. E. Kousky, Observational evidence of Kelvin waves in the tropical stratosphere, *J. Atmos. Sci., 25*, 900-907, 1968.

W. J. Randel, NCAR, P.O. Box 3000 Boulder CO 80307.

(Received August 24, 1989;
revised May 16, 1990;
accepted June 4, 1990.)